Dynamical Systems: An International Journal, Vol. 20, No. 1, March 2005, 149–173

Taylor & Francis
Taylor & Francis Group

Natural and non-natural spacecraft formations near the L_1 and L_2 libration points in the Sun–Earth/Moon ephemeris system

K. C. HOWELL* and B. G. MARCHAND

School of Aeronautics and Astronautics, Purdue University,
315 N. Grant Street, West Lafayette, IN 47907-2023, USA

(*Received 23 April 2004; in final form 14 September 2004*)

Space-based observatory and interferometry missions, such as Terrestrial Planet Finder (TPF), Stellar Imager, and MAXIM, have sparked great interest in multi-spacecraft formation flight in the vicinity of the Sun–Earth/Moon (SEM) libration points. The initial phase of this research considered the formation keeping problem from the perspective of continuous control as applied to non-natural formations. In the present study, closer inspection of the flow corresponding to the stable and centre manifolds near the reference orbit, reveals some interesting natural relative motions as well as some discrete control strategies for deployment. In addition, some implementation issues associated with discrete formation keeping of natural versus non-natural configurations are addressed in the present study.

1. Introduction

Some new concepts for space-based observatories and interferometry missions now incorporate formation flight to meet their objectives [1–4]. Much of the available research on formation flight focuses on Earth orbiting configurations [5–20] where the influence of other gravitational perturbations can be safely ignored. However, renewed interest in formations that evolve near the vicinity of the Sun–Earth libration points has inspired new studies regarding formation keeping in the three-body problem [21–36]. Some of these investigations focus on the simplified circular restricted three-body problem (CR3BP) [28, 30, 32–34]. Previous studies [34] consider linear optimal control, as applied to nonlinear time varying systems, as well as nonlinear control techniques, including input and output feedback linearization. That analysis is initially performed in the CR3BP, but is

*Corresponding author. Email: howell@ecn.purdue.edu

Dynamical Systems: An International Journal
ISSN 1468–9367 print/ISSN 1468–9375 online
http://www.tandf.co.uk/journals
DOI: 10.1080/1468936042000298224

later transitioned into the more complete ephemeris (EPHEM) model [35, 36]. These control strategies are applied to a two spacecraft formation where the chief spacecraft evolves along a three-dimensional periodic halo orbit near the L_2 libration point. The deputy vehicle, through continuous thrusting, is then commanded to follow a non-natural arc relative to the chief.

This particular effort does not constitute the only application of continuous control techniques in the CR3BP. Scheeres and Vinh [28] develop a non-traditional yet innovative continuous controller, based on the local eigenstructure of the linear system, to achieve bounded motion near the vicinity of a halo orbit. Other research efforts have also focused on the effectiveness of continuous control techniques in the general CR3BP, though 'not' in the vicinity of the libration points. Gurfil and Kasdin, for instance, consider both linear quadratic regulator (LQR) techniques [30] and adaptive neural control [33] for formation keeping in the CR3BP. The second approach, described in Gurfil *et al.* [33], incorporates uncertainties introduced by modelling errors, inaccurate measurements, and external disturbances. Luquette and Sanner [32] apply adaptive nonlinear control to address the same sources of uncertainties in the nonlinear CR3BP.

Formations modelled in the CR3BP do represent a good starting point. However, ultimately, any definitive formation keeping studies must be performed in the *n*-body EPHEM model, where the time invariance properties of the CR3BP are lost and, consequently, precisely periodic orbits do not exist near the libration points. Folta *et al.* [27] and Hamilton [31] consider linear optimal control for formation flight relative to Lissajous trajectories, as determined in the EPHEM model. In their studies, the evolution of the controlled formation is approximated from a linear dynamical model relative to the integrated reference orbit. Finally, Howell and Barden [23–25] also investigate formation flying near the vicinity of the libration points in the perturbed Sun–Earth/Moon (SEM) system. Their results are determined in the full nonlinear EPHEM model. Initially, their focus is the determination of the natural behaviour on the centre manifold near the libration points and the first step of their study captures a naturally occurring six-satellite formation near L_1 or L_2 [24]. Further analysis considers strategies to maintain a planar formation of the six vehicles in an orbit about the Sun–Earth L_1 point [23, 25, 26], that is, controlling the deviations of each spacecraft relative to the initial formation plane. A discrete station keeping/control approach is devised to force the orientation of the formation plane to remain fixed inertially. An alternate approach is also implemented by Gómez *et al.* [29] in a study of the deployment and station keeping requirements for the TPF nominal configuration. Their analysis is initially performed in a simpler model but the simulation results are transitioned into the EPHEM model.

In the present study, two types of impulsive control are considered. The first is a basic targeter approach that is, in concept, similar to that implemented by Howell and Barden [23, 25, 26] in the EPHEM model. This particular controller is applied here to an inertially fixed non-natural formation. Also, the station keeping techniques previously implemented by Simó *et al.* [21] and Howell and Keeter [22], based on a Floquet controller, are adapted here to the formation keeping problem. In particular, the Floquet controller is applied to study naturally existing formations near the libration points and the potential deployment into such configurations.

2. Dynamical model

In this investigation, the dynamical model that is employed is based on the standard relative equations of motion for the n-body problem, as formulated in the inertial frame $(\hat{X}-\hat{Y}-\hat{Z})$. The equations are, however, modified to include the effects of solar radiation pressure (SRP). Hence, the dynamical evolution of each vehicle in the formation, relative to the Earth, $\bar{r}^{P_2P_s}$, is governed by

$$ {}^{I}\ddot{\bar{r}}^{P_2P_s} = -\frac{\mu_{P_2}}{\left(r^{P_2P_s}\right)^3} + \sum_{j=1,\, j\neq 2,\, s}^{N} \mu_{P_j}\left(\frac{\bar{r}^{P_sP_j}}{\left(r^{P_sP_j}\right)^3} - \frac{\bar{r}^{P_2P_j}}{\left(r^{P_2P_j}\right)^3}\right) + \bar{f}_{srp}^{(P_s)}. \tag{1} $$

For notational purposes, let P_2 denote the central body of integration, in this case the Earth. Then, P_s represents the spacecraft, and the sum over j symbolizes the presence of other gravitational perturbations. Note that μ_{P_2} and μ_{P_j} represent the gravitational parameters of the central body, P_2, and the jth perturbing body, P_j, respectively. The SRP force vector, as discussed by McInnes [37], is modelled as

$$ \bar{f}_{srp}^{(P_s)} = \frac{kS_0A}{m_sc}\left(\frac{D_0^2}{d^2}\right)\cos^2\beta\,\hat{n}, \tag{2} $$

where k denotes the absorptivity of the spacecraft surface ($k = 2$ for a perfectly reflective surface), S_0 is the energy flux measured at the Earth's distance from the Sun [$\mathrm{W}\cdot\mathrm{m}^{-2}$], D_0 is the mean Sun–Earth distance [km], A represents the constant spacecraft 'effective' cross-sectional area [km^2], c is the speed of light [$\mathrm{km}\cdot\mathrm{s}^{-1}$], m_s is the spacecraft mass [kg], β is the angle of incidence of the incoming photons, $\hat{n}$ denotes the unit surface normal, and d [km] represents the Sun–spacecraft distance.

3. Discrete formation keeping

Based on results from previous investigations [30, 32–36], it appears that it is possible, at least computationally, to achieve precise formations in the CR3BP and in the EPHEM model. That is, 'if' continuous control is both available and feasible. Past studies [34–36] demonstrate that, depending on the constraints imposed on the formation configuration, a continuous control approach may nominally require thrust levels ranging from 10^{-3} to 10^{-9} N. In contrast, the present state of propulsion technology allows for operational thrust levels on the order of 90–1000 μN via pulsed plasma thrusters, such as those available for attitude control onboard EO-1 (http://space-power.grc.nasa-gov/ppo/projects/eo1/eo1-ppt.html). Of course, increased interest in micro- and nano-satellites continues to motivate theoretical and experimental studies to further lower these thrust levels, as discussed by Mueller [38], Gonzalez and Baker [39] and Phipps and Luke [40]. Gonzalez and Baker [39] estimate that a lower bound of 0.3 nN is possible via laser induced ablation of aluminium. Aside from their immediate application to micro- and nano-satellite missions, these concepts are also potentially promising for formation flight near the libration points.

Ultimately, the level of accuracy achievable in tracking the nominal motion, for a given configuration, depends strongly on the ability to deliver the required thrust levels accurately. Although continuous control approaches are mathematically

sound, the science goals of deep space missions may impose a series of constraints that eliminate continuous control as a feasible option. Some also suggest that maintaining a precise formation is, perhaps, ultimately not as critical as generating precise knowledge of the relative position of each spacecraft in the formation. In these cases, a discrete formation keeping strategy may represent an important capability.

3.1 *Investigation of various discrete control strategies*

In this study, two discrete control strategies are considered for formation keeping. Both of these rely on knowledge of the linearized dynamics associated with the reference orbit, but incorporate the nonlinear response of the vehicle. In this case, the reference orbit is the path of the chief spacecraft, assumed to evolve along a 2×10^5 km halo orbit, as determined in the SEM ephemeris system. The deputy dynamics, then, are modelled as a perturbation relative to the reference orbit. The success of a particular control strategy depends, in part, on the nominal motion that is required of the deputy.

In the first method, a simple linear targeter is applied to enforce a non-natural formation. In particular, the nominal path of the deputy spacecraft is characterized as an inertially fixed distance and orientation, relative to the chief spacecraft. Since this type of motion does not exist naturally near the libration points, continuous control is necessary to 'precisely' enforce the formation for the duration of the mission. It is assumed that the goals of the mission require formation keeping accuracies below 10^{-3} m. Here, instead of applying continuous control, the path of the deputy is divided into segments. At the beginning of each segment, an impulsive manoeuvre is implemented that targets the nominal state at the end of the segment. If the nominal separation between the chief and deputy spacecraft is small, this approach proves to be effective if the required tolerances are on the order of 10^{-2} m. Whether this represents an acceptable tolerance level depends on the goals of the mission. For instance, as presently envisioned, missions like Stellar Imager require that the nominal vehicle configuration be maintained to within 10^{-6} m. The results from earlier studies [34–36] clearly indicate, then, the need for continuous formation control if non-natural relative motions are of interest.

Alternatively, a controller derived from Floquet analysis, based on the reference orbit, is designed to remove the unstable component of the relative state, as well as two of the four centre subspace modes that are associated with the reference orbit. The path of the deputy, then, is representative of a synthesis between the stable and centre flows. In contrast with the first method, this type of control does 'not' target a non-natural reference motion. Instead, the control scheme nominally places the deputy spacecraft on a naturally existing path that exhibits nearly periodic behaviour, bounded motion, or quasi-periodic motion relative to the chief spacecraft. The control essentially seeks to return the deputy to this natural path.

4. Discrete control of non-natural formations in the ephemeris model

Driven by control and/or implementation requirements, some new consideration is warranted concerning the degree of accuracy to which the formation can be maintained via discrete impulses. A discrete LQR controller yields the optimal magnitude for each differential control impulse at specified time intervals. This approach is

suitable for station keeping of natural solutions, such as Lissajous trajectories or halo orbits, which nominally require no control. However, non-natural solutions do require a nominal control input. The value of the nominal control input that must be added is still assumed to be continuously available. Hence, the LQR method, in this case, does not yield a truly discrete formation keeping strategy.

4.1 *Targeting a nominal relative state*

Consider a formation where the chief spacecraft evolves along the Lissajous trajectory plotted in figure 1, near the SEM L_2 point. Note that this trajectory is determined in the EPHEM model. Furthermore, let the nominal state of the deputy be defined by the position vector $\bar{\rho}(t)$, measured from the chief to the deputy, and the relative velocity vector $\dot{\bar{\rho}}(t)$. In the present example, $\bar{\rho}(t) = (100\,\text{km})\hat{Y}$ and $\dot{\bar{\rho}}(t) = \bar{0}$. Since this type of 'relative' spacecraft motion is not consistent with the natural dynamics near the libration points, at least nearly continuous control is necessary for precise formation keeping. However, if the mission specifications allow some flexibility in the relative vehicle position tolerances, an impulsive control approach may be sufficient. The impulsive scheme presented here is based on a differential corrections approach.

Consider the general form of the solution to the linear system

$$\begin{bmatrix} \delta\bar{r}_{k+1} \\ \delta\dot{\bar{r}}_{k-1}^{-} \end{bmatrix} = \Phi(t_{k-1}, t_k) \begin{bmatrix} \delta\bar{r}_k \\ \delta\dot{\bar{r}}_k^{+} \end{bmatrix} = \begin{bmatrix} A_k & B_k \\ C_k & D_k \end{bmatrix} \begin{bmatrix} \delta\bar{r}_k \\ \delta\dot{\bar{r}}_k^{-} + \Delta\bar{V}_k \end{bmatrix}, \tag{3}$$

where $\Phi(t_{k+1}, t_k)$ denotes the state transition matrix, from time t_k to time t_{k+1}, associated with the 'actual' deputy spacecraft path. The symbol δ denotes a perturbation relative to the actual deputy path and $\Delta\bar{V}_k$ represents an impulsive manoeuvre applied at the beginning of the kth segment, marked by t_k. In this case, $\delta\bar{r}_k = \bar{r}_k^{\circ} - \bar{r}_k$, $\delta\dot{\bar{r}}_k^{-} = \dot{\bar{r}}_k^{\circ} - \dot{\bar{r}}_k^{-}$, and $\delta\bar{r}_{k+1} = \bar{r}_{k+1}^{\circ} - \bar{r}_{k+1}$ where the superscript '$\circ$' denotes evaluation along the nominal deputy path. That is, $\bar{r}_k^{\circ} = \bar{r}^{P_2C}(t_k) + \bar{\rho}^{\circ}(t_k)$ and $\dot{\bar{r}}_k^{\circ} = \dot{\bar{r}}^{P_2C}(t_k) + \dot{\bar{\rho}}(t_k)$, where '$P_2C$' denotes the distance from P_2 to the chief spacecraft. Controlling the position of the deputy spacecraft relative to the chief to a constant vector, as observed in the inertial frame, is equivalent to targeting a particular constant perturbation in position, $\delta\bar{r}_{k+1}$, relative to the inertial frame. An impulsive manoeuvre of the form

$$\Delta\bar{V}_k = B_k^{-1}(\delta\bar{r}_{k+1} - A_k\delta\bar{r}_k) - \delta\dot{\bar{r}}_k^{-}, \tag{4}$$

will accomplish the goal in the linear system. In the nonlinear EPHEM model employed here, a precise implementation of this scheme is accomplished through a differential corrections process performed over each segment, as discussed by Howell and Barden [23, 25, 26]. A sample implementation of this approach, in the EPHEM model, is presented in figure 2. The manoeuvre strategies associated with each curve in figure 2 are illustrated in figure 3. Note, from figure 2, that during the wait period between manoeuvres the trajectory diverges quickly from the prespecified nominal path. Naturally, the maximum error incurred along each segment decreases as the scheduled time between manoeuvres decreases. In spite of this trend, these results indicate that, if the nominal radial separation is large, continuous control is still required if a good level of accuracy is desired.

Smaller formations, on the other hand, may benefit from a discrete approach. For instance, consider a formation characterized by $\bar{\rho} = (10\,\text{m})\hat{Y}$ and $\dot{\bar{\rho}} = \bar{0}$. As

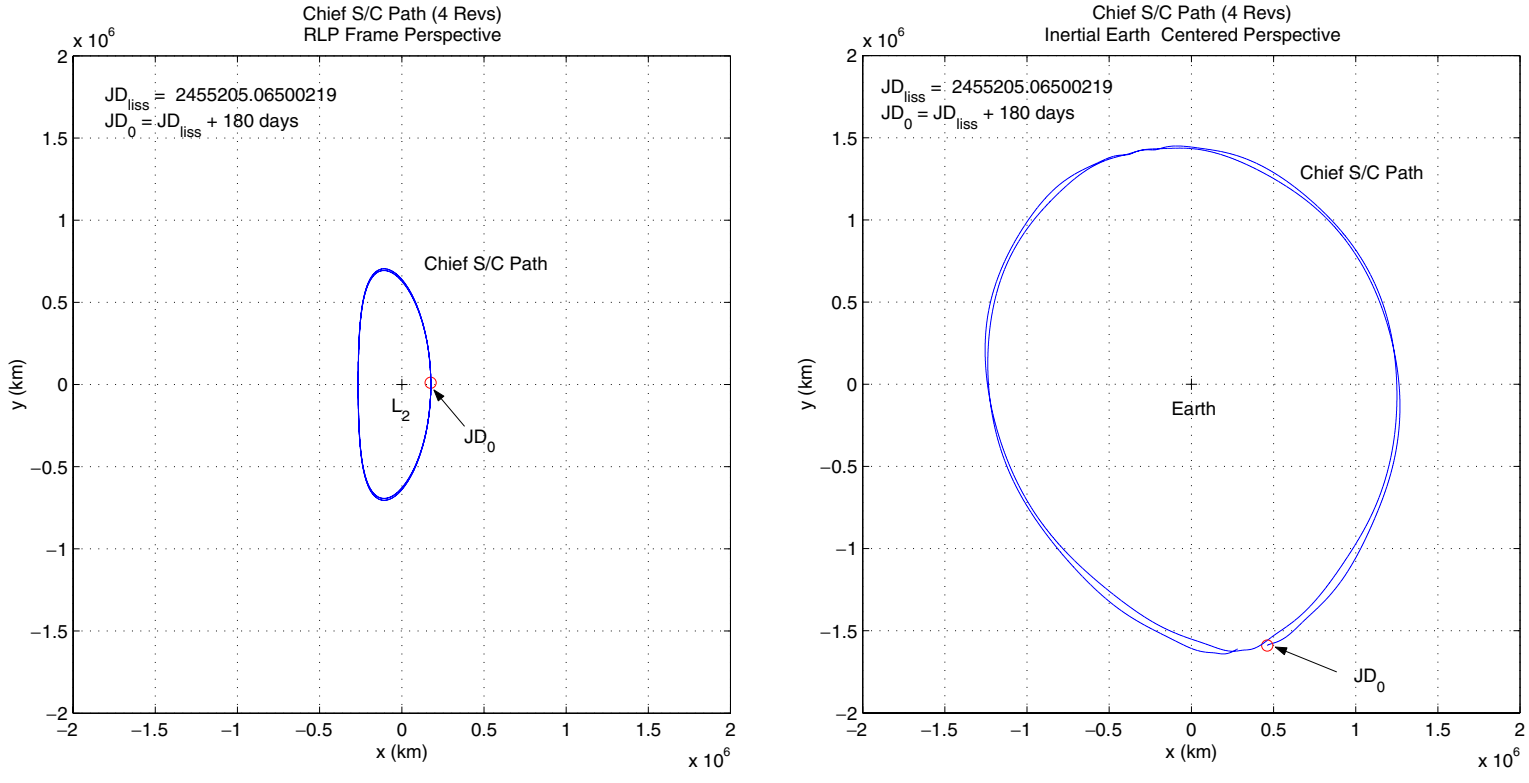

Figure 1. Reference Lissajous trajectory for chief spacecraft (s/c) path (rotating and inertial frame perspectives).

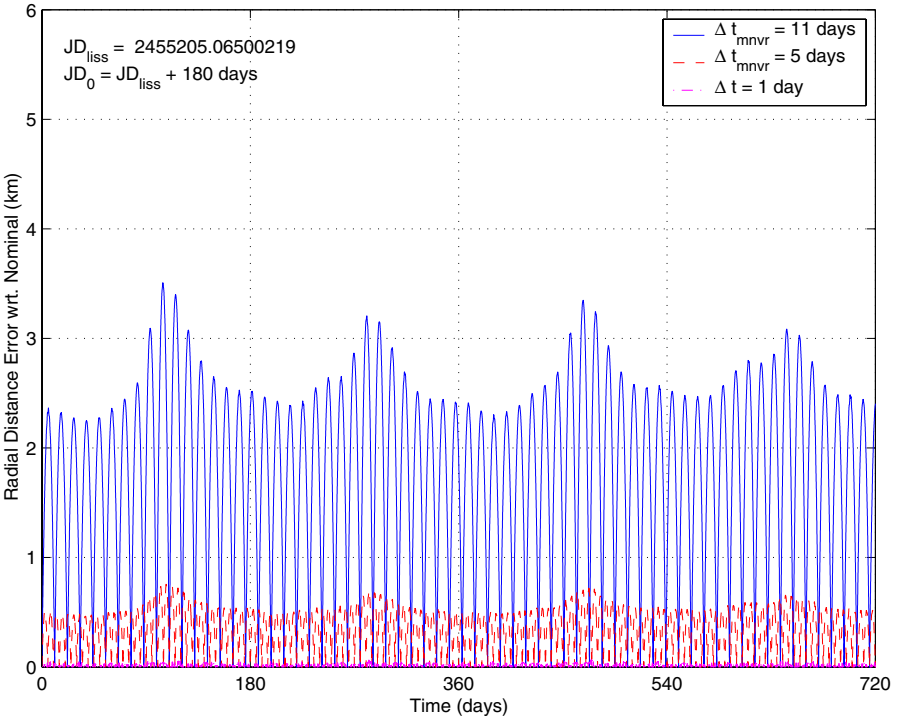

Figure 2. Position error relative to the nominal path for various manoeuvre intervals over two Earth cycles.

depicted in figure 4, the maximum distance deviation between manoeuvres is significantly smaller, dropping below 10^{-2} m for manoeuvres scheduled at least every 2 days. However, the magnitude of the individual manoeuvres, illustrated in figure 5, has decreased by several orders of magnitude, compared to the manoeuvres in figure 3. In practice, the error introduced in any attempt to physically implement such small manoeuvres may offset the benefits. In addition, the tolerances achievable with any impulsive approach, for a fixed manoeuvre schedule, depends on the nominal separation between the vehicles. As observed from figure 6, formation separations of up to 50 m can be achieved to within 10^{-2} m at all times, if a manoeuvre is performed once a day. If that interval is doubled to once every 2 days, then the maximum relative separation recommended drops to 15 m.

Clearly, achieving the desired nominal configuration to extreme accuracy requires manoeuvres that are fairly close to each other. As previously mentioned, as the manoeuvres become more closely spaced they also decrease in size. Note that the magnitude of the manoeuvres illustrated in figure 5 is already extremely small (10^{-6} m s^{-1}). So, regardless of whether continuous or discrete control is available, accurately maintaining a 'non-natural' nominal configuration, with small relative separations, still requires very low thrust capabilities [38–41]. Delivering such small control inputs, accurately, may or may not be achievable with the technology presently available. Whether or not that is true depends on the required nominal path, any dynamical or mission specific constraints imposed on the formation, and the sensitivity

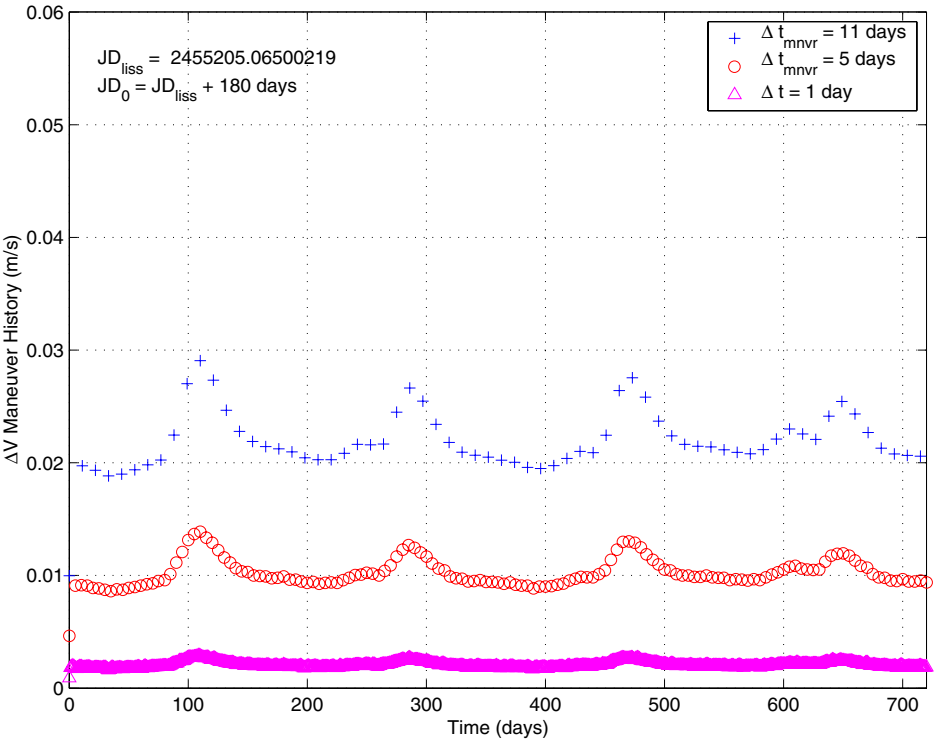

Figure 3. Station keeping manoeuvre strategy for a 100 km two spacecraft formation aligned with inertial y-axis.

of this analysis to modelling and measurement uncertainties as well as thrust implementation errors. Since the natural flow in this region of space is constantly acting against these non-natural configurations, the relative error can increase rapidly if these small manoeuvres are not accurately implemented. Conversely, formations that take advantage of the natural flow near the reference orbit require minimal station keeping beyond the initial injection manoeuvre.

5. Formations that exploit the centre + stable manifolds

The centre manifold that exists near the libration points allows for a variety of natural motions that could prove beneficial for formation flight. Lissajous trajectories and halo orbits are examples of motions that exist within the centre manifold near L_1 and L_2. A Lissajous trajectory, for instance, allows for a phased natural formation whose geometry is analogous to a 'string of pearls'. To illustrate the concept, consider the Lissajous trajectory represented in figure 7. The blue surface in figure 7 is traced by a quasi-periodic Lissajous trajectory near the SEM L_2 point, as determined in the SRP perturbed n-body EPHEM model. By properly phasing each vehicle, it is possible for the formation to naturally evolve along this surface such that the relative positions of each spacecraft in the formation are unaltered and the relative distances are closely bounded. That is, if the formation originates as a string of pearls, the orientation of the string is relatively unaffected in time,

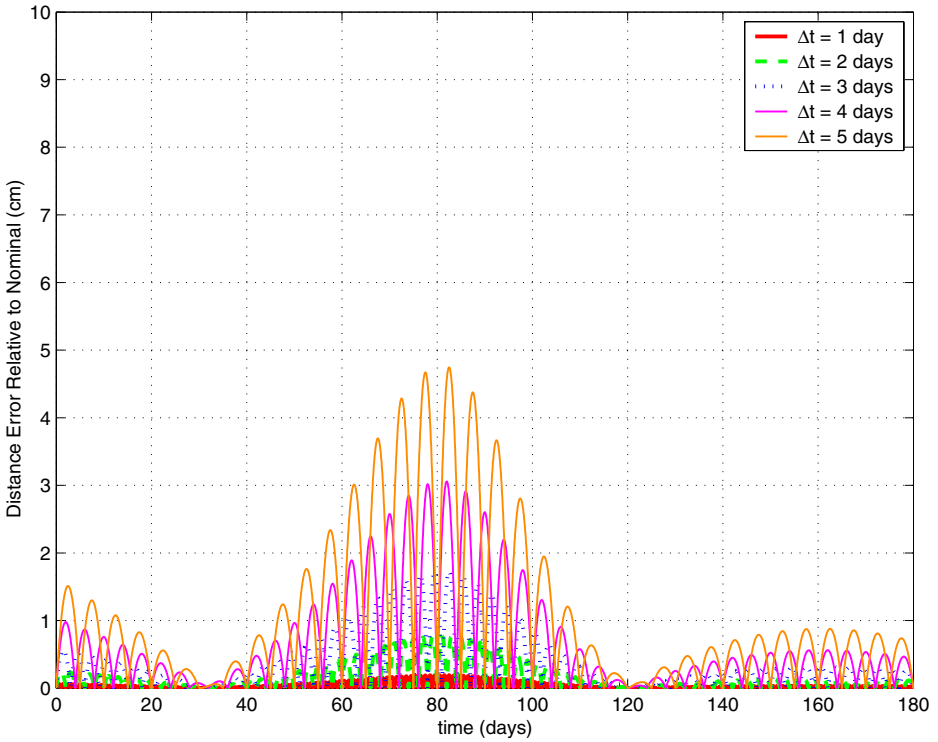

Figure 4. Position error relative to the nominal path as a function of the length of the manoeuvre interval.

the lead vehicle always remains in the lead and the order of each subsequent vehicle along the 'string of pearls' remains unchanged.

Since each spacecraft in this formation evolves along a naturally existing Lissajous trajectory, maintaining this type of formation can be achieved with a standard station keeping approach. Other relative motions can be numerically identified through a linear stability analysis of a reference solution near the libration points, such as a halo orbit in the CR3BP. The process of identifying these relative motions requires an understanding of the eigenstructure associated with the reference orbit. To that end, the analysis of the centre manifold as presented here employs the CR3BP, where the reference orbit is defined as a three-dimensional, periodic halo orbit. The natural formation dynamics in the vicinity of the reference orbit are studied in detail. Once a suitable set of nominal configurations is identified, the results are easily transitioned into the EPHEM model previously described via a differential corrections process.

5.1 *Floquet analysis*

Let $\bar{x}^*(t)$ denote the state vector, at time t, along a reference halo orbit near L_1 or L_2 in the CR3BP and let $\delta\bar{x}(t)$ denote a perturbation relative to $\bar{x}^*(t)$. Since the following analysis is performed in the CR3BP, these vectors are both expressed in terms of rotating coordinates consistent with the standard definition of the synodic rotating frame. In this frame, $\hat{x}$ is directed from the Sun to the Earth/Moon barycentre,

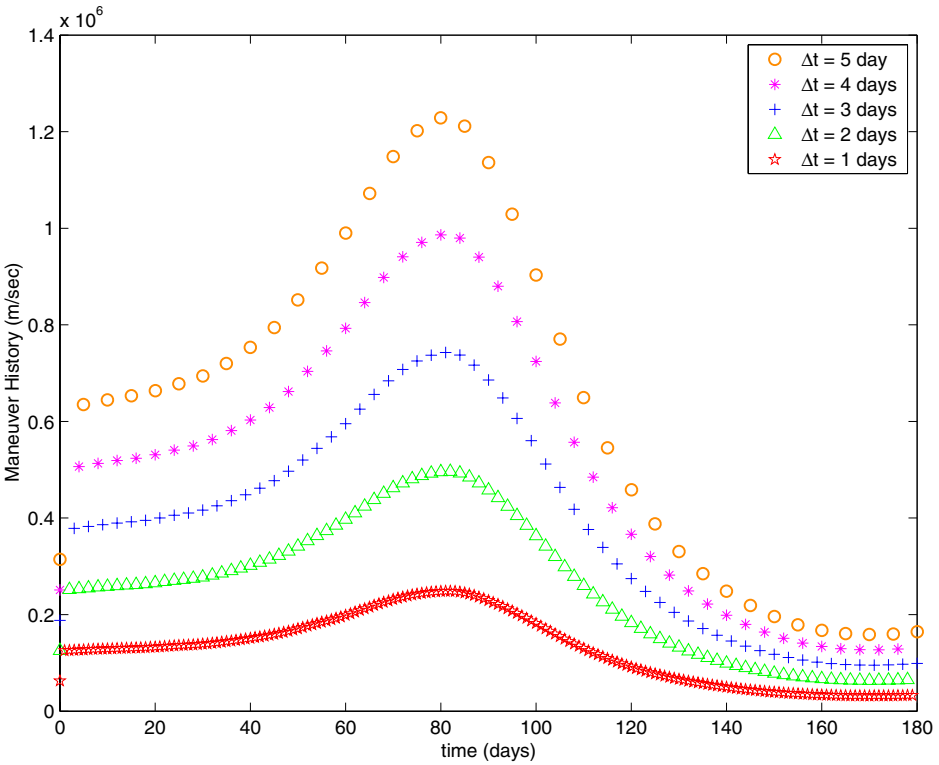

Figure 5. Station keeping manoeuvre strategy (10 m two spacecraft formation aligned with inertial y-axis).

$\hat{z}$ is normal to the plane of motion of the primaries, and $\hat{y}$ completes the right-handed triad. The velocity elements of the vectors $\bar{x}^*(t)$ and $\delta\bar{x}(t)$ are both associated with an observer fixed in the rotating frame.

In terms of the linearized dynamics, the evolution of the perturbation vector $\delta\bar{x}(t)$ is governed by the state transition matrix, $\Phi(t,0)$, such that

$$\delta\bar{x}(t) = \Phi(t,0)\delta\bar{x}(0). \tag{5}$$

Since the reference orbit is T-periodic, the state transition matrix admits a Floquet decomposition [42] of the form

$$\Phi(t,0) = \{P(t)S\}e^{Jt}\{P(0)S\}^{-1}, \tag{6}$$

where $P(t) = P(t+T)$ is a periodic matrix, $P(0)$ is the identity matrix, and J is a block diagonal matrix formed by the real and imaginary parts of the Floquet exponents (γ_j) of $\Phi(T,0)$. The reference halo orbits of interest in this study are inherently unstable and characterized by a first-order instability. That is, $\gamma_1 > 0$, $\gamma_2 < 0$, γ_3 and γ_4 are purely imaginary, and $\gamma_5 = \gamma_6 = 0$. The columns of S represent the real and imaginary parts of the Floquet modes ($\bar{s}_j$). The Floquet Modal matrix is subsequently defined as

$$E(t) = P(t)S = \Phi(t,0)E(0)e^{-Jt}. \tag{7}$$

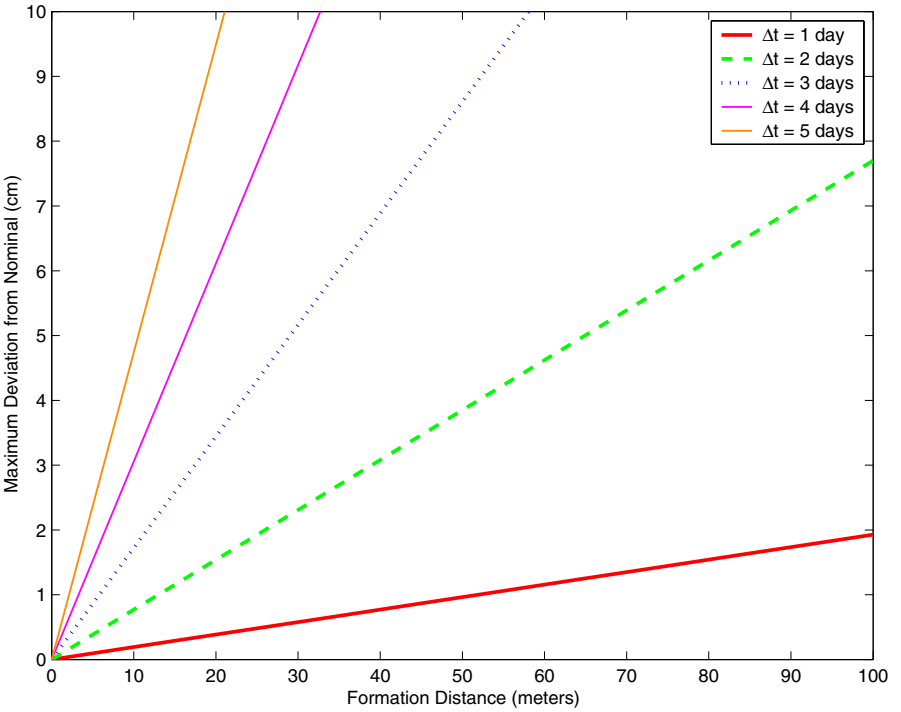

Figure 6. Maximum radial deviation as a function of nominal formation distance and manoeuvre time interval.

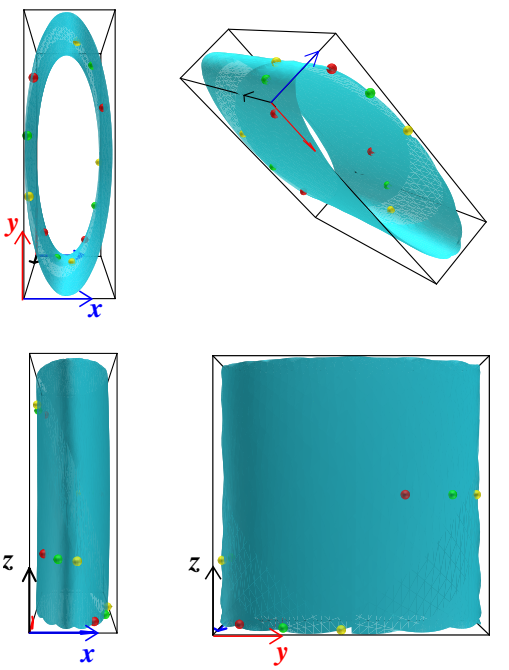

Figure 7. Natural 'string of pearls' formation in the EPHEM model.

Note that, since $P(t)$ is periodic, and S is a constant matrix, $E(t) = E(t+T)$ and $E(0) = S$. The Floquet modes at each point along the reference orbit can be computed from equation (7). Now, at a point in time, the perturbation $\delta\bar{x}(t)$ can be expressed in terms of any six-dimensional basis. The Floquet modes ($\bar{e}_j$), defined by the columns of $E(t)$, form a non-orthogonal six-dimensional basis. Hence, $\delta\bar{x}(t)$ can be expressed as

$$\delta\bar{x}(t) = \sum_{j=1}^{6} \delta\bar{x}_j(t) = \sum_{j=1}^{6} c_j(t)\bar{e}_j(t), \tag{8}$$

where $\delta\bar{x}_j(t)$ denotes the component of $\delta\bar{x}(t)$ along the jth mode, $\bar{e}_j(t)$, and the coefficients $c_j(t)$ are easily determined as the elements of the vector $\bar{c}(t)$ defined by

$$\bar{c}(t) = E(t)^{-1}\delta\bar{x}(t). \tag{9}$$

The Floquet analysis presented above is implemented by Howell and Keeter [22], based on work originally performed by Simó *et al.* [21], as the basis of a station keeping strategy for a single spacecraft evolving along a halo orbit. In their study, Howell and Keeter (following [21]) determine the impulsive manoeuvre scheme that is required to periodically remove the unstable component, $\delta\bar{x}_1$, of the perturbation, $\delta\bar{x}(t)$. In the present analysis, a similar approach is employed to remove the component of $\delta\bar{x}$ that is associated with the unstable mode as well as two of the four centre modes. Thus, the control will eliminate three components. To illustrate this, let

$$\delta\bar{x}(t)^{\circ} = \sum_{\substack{j=2,3,4 \text{ or} \\ j=2,5,6}} (1+\alpha_j(t))\delta\bar{x}_j, \tag{10}$$

denote the 'desired' perturbation relative to the reference orbit, where the $\alpha_j(t)$ denote some yet to be determined coefficients. The control problem, then, reduces to finding the impulsive manoeuvre, $\Delta\bar{V}(t)$, such that

$$\sum_{\substack{j=2,3,4 \text{ or} \\ j=2,5,6}} (1+\alpha_j(t))\delta\bar{x}_j(t) = \sum_{j=1}^{6} \delta\bar{x}_j + \begin{bmatrix} 0_3 \\ \Delta\bar{V} \end{bmatrix}. \tag{11}$$

Let $\delta\bar{x}_{jr}$ denote the first three elements of the vector $\delta\bar{x}_j$, $\delta\bar{x}_{jv}$ the last three elements of $\delta\bar{x}_j$, and $\bar{\alpha}$ represent a 5×1 vector formed by the α_j coefficients in equation (11). Then, the $\Delta\bar{V}$ required to remove modes $\bar{e}_1$, $\bar{e}_3$, and $\bar{e}_4$ is computed as

$$\begin{bmatrix} \bar{\alpha} \\ \Delta\bar{V} \end{bmatrix} = \begin{bmatrix} \delta\bar{x}_{2\bar{r}} & \delta\bar{x}_{5\bar{r}} & \delta\bar{x}_{6\bar{r}} & 0_3 \\ \delta\bar{x}_{2\bar{v}} & \delta\bar{x}_{5\bar{v}} & \delta\bar{x}_{6\bar{v}} & -I_3 \end{bmatrix}^{-1} (\delta\bar{x}_1 + \delta\bar{x}_3 + \delta\bar{x}_4). \tag{12}$$

Similarly, the $\Delta\bar{V}$ required to remove modes $\bar{e}_1$, $\bar{e}_5$, and $\bar{e}_6$ is exactly determined from

$$\begin{bmatrix} \bar{\alpha} \\ \Delta\bar{V} \end{bmatrix} = \begin{bmatrix} \delta\bar{x}_{2\bar{r}} & \delta\bar{x}_{3\bar{r}} & \delta\bar{x}_{4\bar{r}} & 0_3 \\ \delta\bar{x}_{2\bar{v}} & \delta\bar{x}_{3\bar{v}} & \delta\bar{x}_{4\bar{v}} & -I_3 z \end{bmatrix}^{-1} (\delta\bar{x}_1 + \delta\bar{x}_5 + \delta\bar{x}_6). \tag{13}$$

Either one of these controllers leads to motion that exhibits not only the overall features of the associated centre subspaces, but also some of the features more commonly associated with motion along a stable manifold. As a direct result, the controllers described by equations (12) and (13) not only define other potential

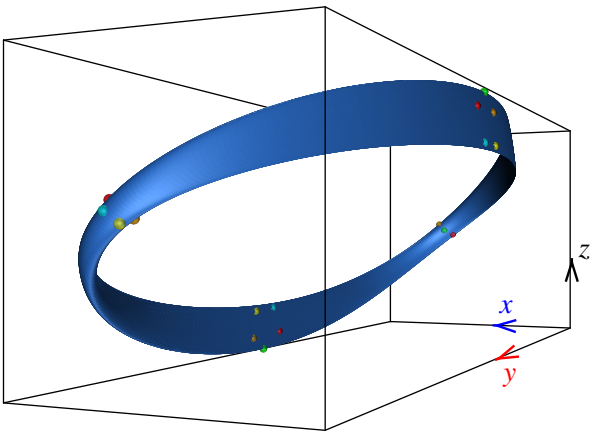

Figure 8. Six spacecraft formation evolving along two-dimensional torus near L_1 in the SEM EPHEM model.

nominal configurations, but also deployment into these configurations, as is demonstrated below.

In general, centre modes are indicative of the existence of additional bounded solutions in the vicinity of the reference orbit. For instance, modes $\bar{e}_3(t)$ and $\bar{e}_4(t)$ span a two-dimensional subspace associated with solutions that evolve along a hollow two-dimensional (2D) torus, known to envelop the halo orbit, as illustrated in figure 8. This type of torus exists both in the CR3BP and in the EPHEM model and represents a natural (unforced) solution to the nonlinear equations of motion. In fact, the solution illustrated in figure 8 is associated with the EPHEM model. Hence, if the initial perturbation, $\delta\bar{x}(0)$, is entirely contained within the subspace spanned by $\bar{e}_3$ and $\bar{e}_4$, then the perturbed path, relative to the halo orbit, is bounded and evolves along a torus, such as that illustrated in figure 8.

Now, suppose that $\delta\bar{x}(t)$ represents the relative dynamics of a deputy spacecraft. This implies that the chief spacecraft is assumed to evolve along the halo orbit. The relative path that defines the motion of the deputy is best visualized from figure 9. Relative to the chief spacecraft, figure 9 depicts, as a surface, the trajectory along which the deputy evolves. In this depiction, the chief spacecraft is always located at the origin. Note that the solution in figure 9 is self-intersecting, but that is merely a product of the projection of the six-dimensional states onto three-dimensional configuration space. Furthermore, although the solution illustrated in figure 9 is generated in the linear system, it is known to represent a natural solution to the nonlinear equations both in the CR3BP and in the EPHEM model, as illustrated in figure 8.

5.2 *Application: Floquet controller to deploy into quasi-periodic torus formation*

Consider a two spacecraft formation where the chief spacecraft is assumed to evolve along a 2×10^5 km halo orbit near the SEM L_1 point. Both spacecraft are deployed and arrive simultaneously at different points along the *xz*-plane. Let the 'arrival' point for both spacecraft be defined as the point where they cross the *xz*-plane near the reference orbit. The position of the deputy spacecraft upon arrival is similar to

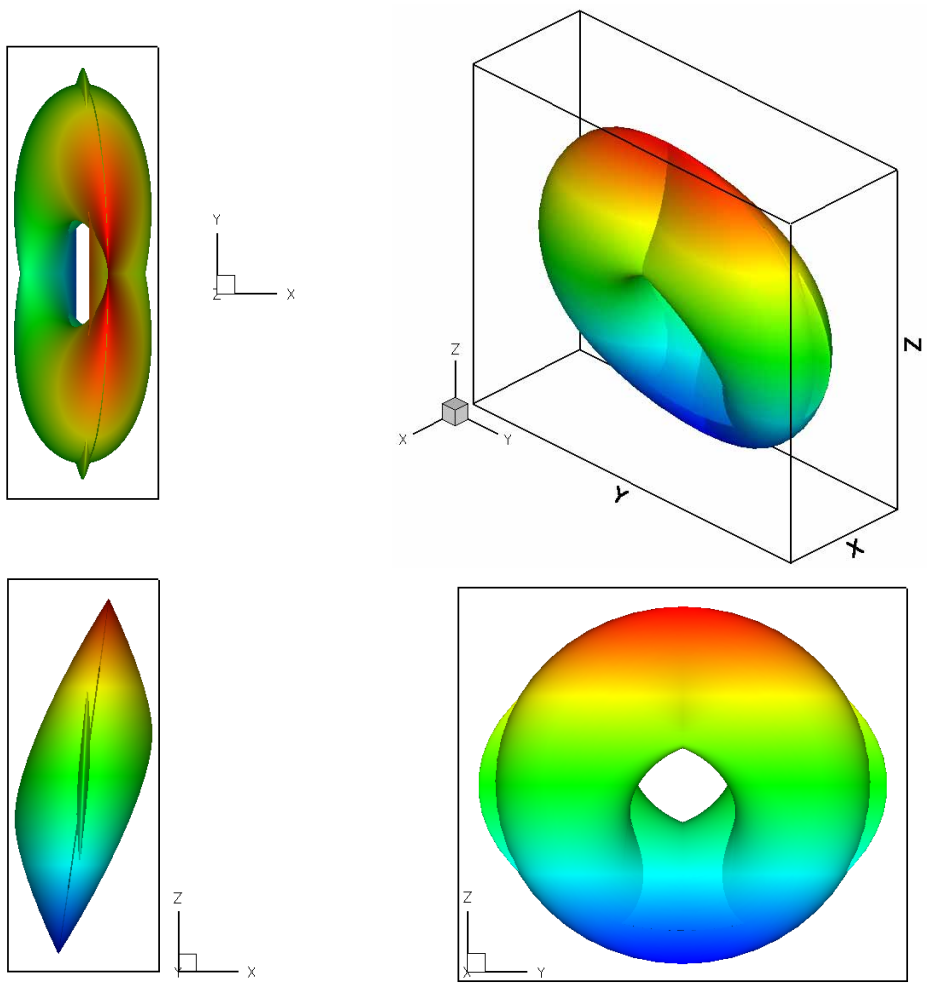

Figure 9. Relative deputy motion along centre manifold.

the chief but 50 m off along the $+\hat{x}$-direction. The relative velocity of the deputy is not important, only the relative orientation of the two spacecraft is relevant.

Once at the arrival point, the deputy spacecraft performs its first formation keeping manoeuvre, as determined from equation (13). This manoeuvre is the largest and is meant to place the spacecraft state into the desired subspaces. The magnitude of the manoeuvre is approximately equal to the magnitude of the relative velocity of the deputy with respect to the chief. For this particular example, the initial relative velocity of the deputy is selected as $\dot{\bar{r}}(0) = (\hat{x} - \hat{y} + \hat{z})\,\mathrm{m\,s^{-1}}$. Thus, the first manoeuvre of the deputy vehicle is $|\Delta \bar{V}_1| = 1.73\,\mathrm{m\,s^{-1}}$. Thereafter, the trajectory of both the chief and deputy spacecraft requires a small deterministic $\Delta \bar{V}$ every 180 days (one orbital period along the halo orbit). For the chief spacecraft, these are necessary to enforce the periodicity condition over 100 orbital periods (and may simply be a numerical artefact). All of these corrections—both for the chief and deputy—are on the order of $10^{-8}\,\mathrm{m\,s^{-1}}$. The resulting path is illustrated in figure 10. The first leg

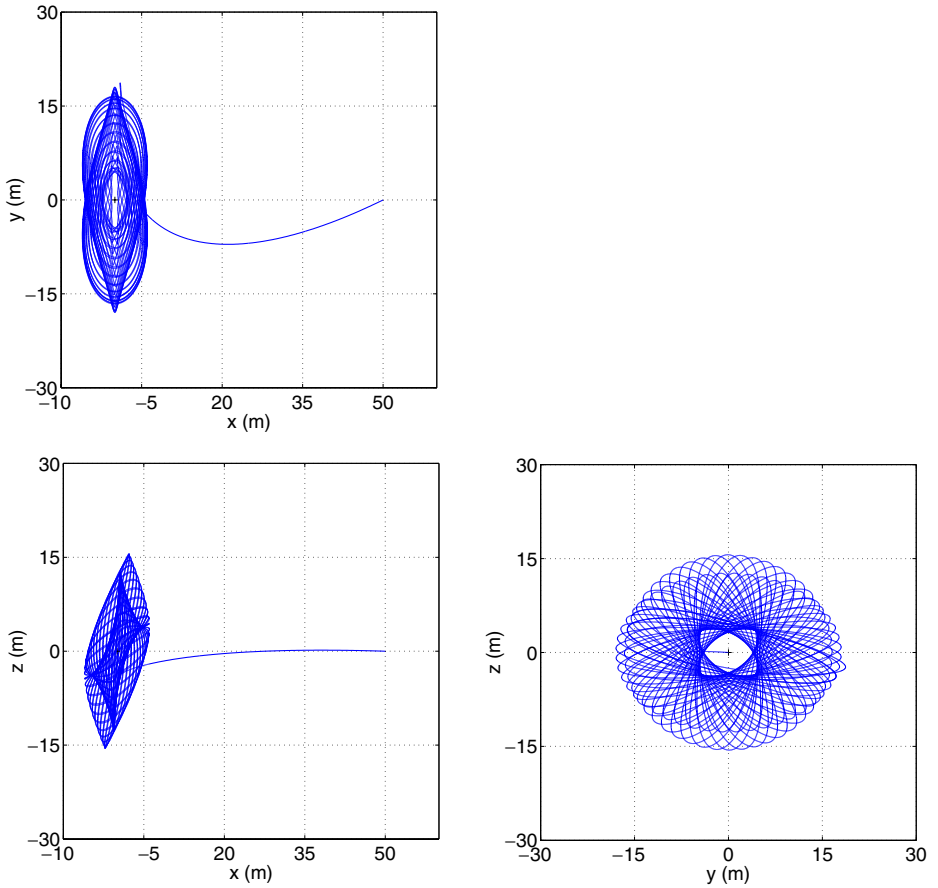

Figure 10. Deployment into toroidal formation (initial state excites only modes five and six).

of the path is characteristic of motion associated with mode two, that is, the stable mode, while the converged path is consistent with the motion associated with modes five and six, previously illustrated in figure 9.

5.3 *Application: Floquet controller to deploy into nearly periodic formations*

For the same reference halo orbit employed in the previous example, consider three deputies deployed along with the chief spacecraft. Each deputy spacecraft arrives simultaneously at a different location relative to the chief. In particular, the relative position vectors are 50, 100, and 140 m along the $+x$-direction. Application of the Floquet controller described by equation (2) leads to a nearly periodic formation.

Once again, the first leg along the path of each deputy resembles motion along the stable manifold associated with the reference halo orbit. However, the converged path is nearly periodic, as observed from figure 11. The resulting path is propagated in the figure for 10 revolutions of the reference halo orbit (1800 days). Beyond

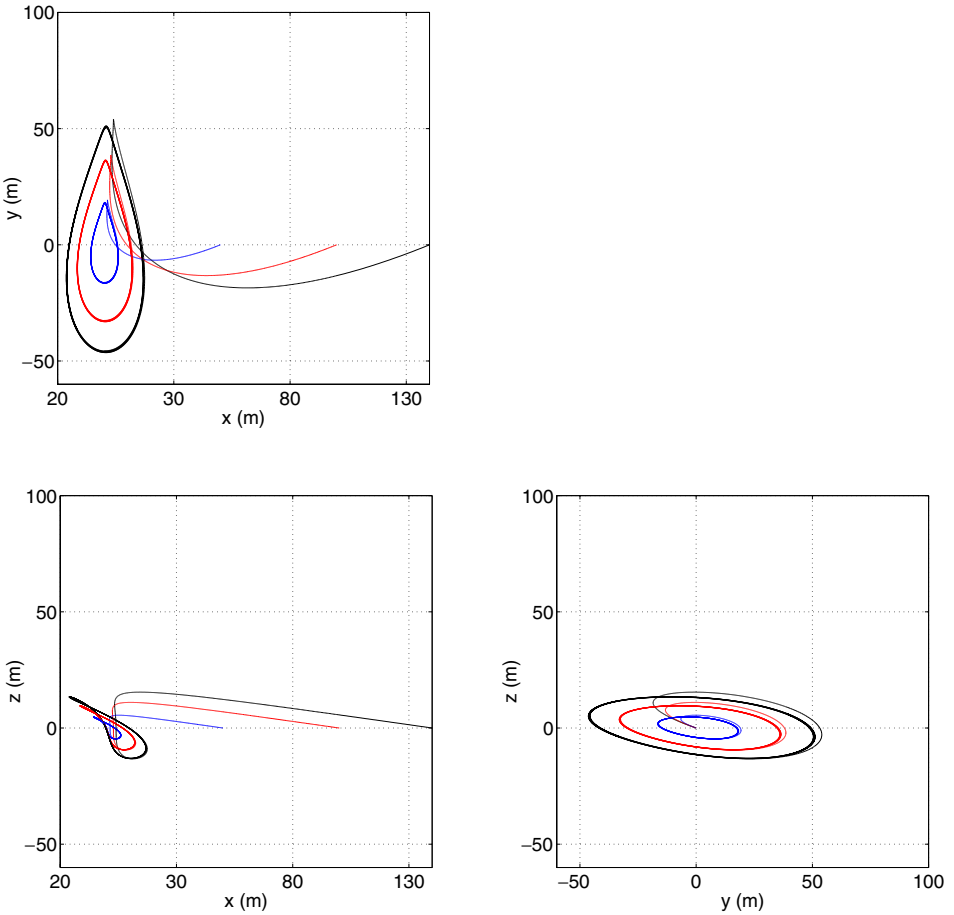

Figure 11. Deployment into nearly periodic formation (initial state excites only modes three and four).

the initial injection manoeuvre, numerical corrections are implemented once every 180 days, although the magnitude is small ($10^{-8}\,\mathrm{m\,s^{-1}}$).

The converged segment of the path in figure 11 reveals a variety of nearly periodic solutions in the vicinity of the chief spacecraft. Since the controller forces these solutions to remain within a subspace spanned by $\bar{e}_2$, $\bar{e}_5$, and $\bar{e}_6$, the resulting path is not evolving solely along the halo family but rather along another type of nearly periodic motion in the vicinity of the reference halo orbit. This is most apparent as the amplitude of the relative orbits is increased above 10^3 km. To better visualize the potential configurations, figure 12 illustrates eight deputies evolving along these nearly periodic orbits. Depending on the desired orbit amplitude, the actual path of each vehicle expands away from the chief spacecraft, but at a very slow rate. So, the individual orbits can be propagated for 100 revolutions of the reference halo, in the CR3BP, and will still appear periodic if the relative separations are small.

Let $\bar{r}(t)$ denote the vector formed by the position elements of $\delta\bar{x}(t)$. The orbits depicted in figure 12 are obtained by applying the controller to a relative position

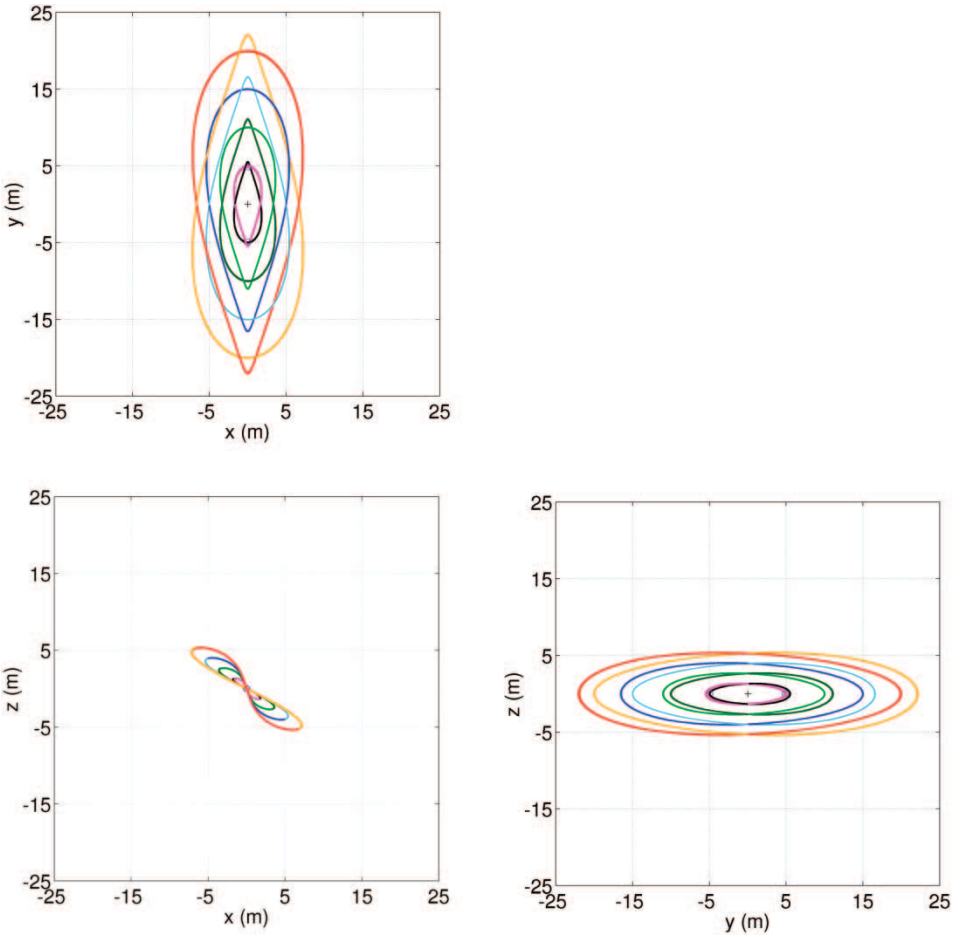

Figure 12. Natural eight spacecraft formation about a single chief spacecraft.

vector of the form $\bar{r}(0) = r_0\,\hat{y}$, where r_0 denotes some initial separation between the chief and deputy spacecraft. The rate of expansion of these orbits is more noticeable if the initial position vector originates anywhere else in the yz-plane. In fact, the rate of expansion reaches a maximum if the initial relative position vector is of the form $\bar{r}(0) = r_0\hat{z}$. In this case, the resulting orbits appear nearly vertical and are illustrated in figure 13 using a four spacecraft formation as an example. In the yz-projection, it is apparent that the expansion proceeds clockwise since, in this case, the reference orbit is a northern L_1 halo orbit. This is consistent with the direction of motion both along the halo family and the stable manifold in this region of space.

Figure 14 further illustrates how the rate of expansion changes as the initial state is shifted throughout the yz-plane. The relative deputy paths illustrated in figure 14(a) are determined in the CR3BP, based on the Floquet analysis previously discussed. These trajectories serve as an initial guess to a two-level differential corrections process, developed by Howell and Pernicka [43], used to numerically identify the equivalent solutions in the EPHEM model. The solutions associated with the SRP perturbed EPHEM model are illustrated in figure 14(b). The sphere at the origin (the location of the chief) is included only to aid in visualizing the path of the deputy.

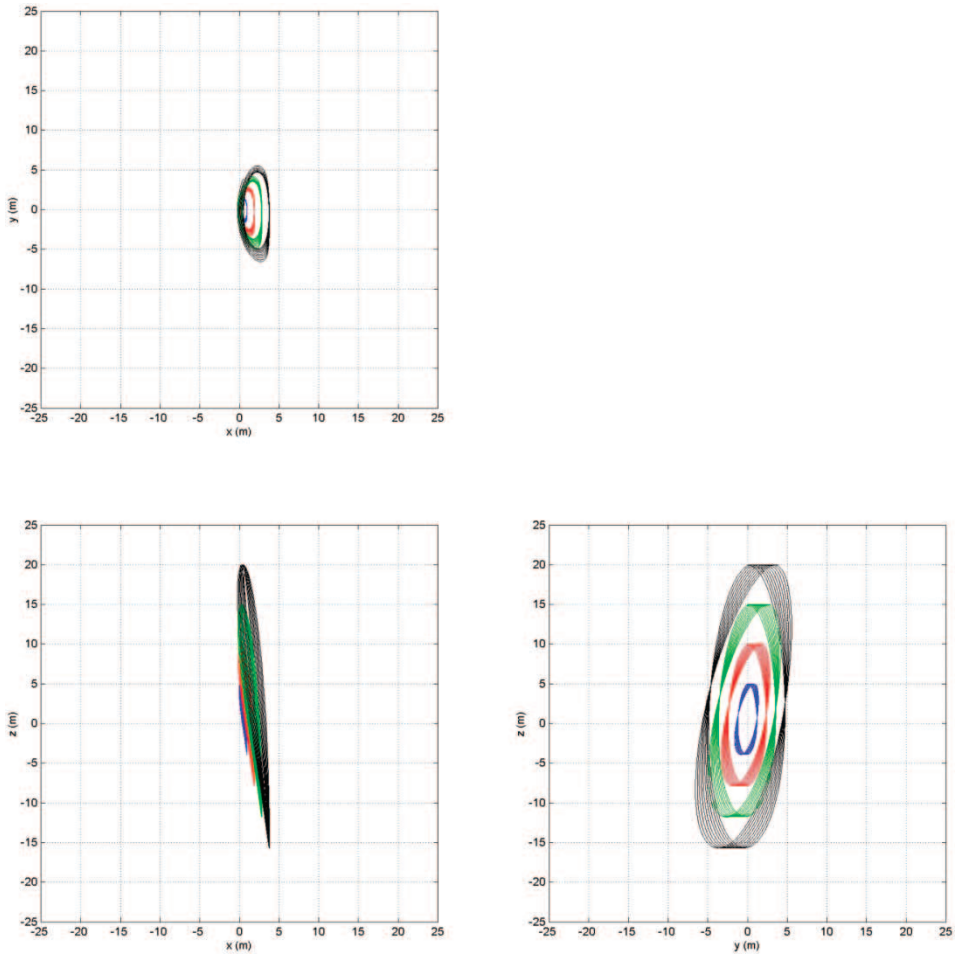

Figure 13. Nearly vertical relative orbits (four spacecraft formation).

Note that with no initial z-component, the orbit of the vehicle is periodic in the CR3BP and nearly periodic in the EPHEM model. As an out-of-plane component is introduced into the initial state, the resulting trajectory blends the characteristics of the orbits in both figures 12 and 13. Further propagating a nearly vertical orbit, characterized by $\bar{r}(0) = r_0\,\hat{z}$, over a period of 100 revolutions (49.2 years) yields the surface illustrated in figure 15.

These naturally existing motions can be used as initial guesses to compute non-natural formations. For instance, consider the sample relative deputy trajectories plotted in figure 16(a)–(c). These trajectories are determined in the EPHEM model both with and without SRP. For each of these examples, the deputy path is clearly not periodic but, the initial guess is sufficiently close to periodic if the effects of SRP are small. In this case, a differential corrector can be applied to enforce periodicity if impulsive manouvres are allowed. The process is similar to a method commonly used to transition halo orbits into the EPHEM model. Consider the first two revolutions of the path (without SRP) in figure 16(b). A two-level differential corrections

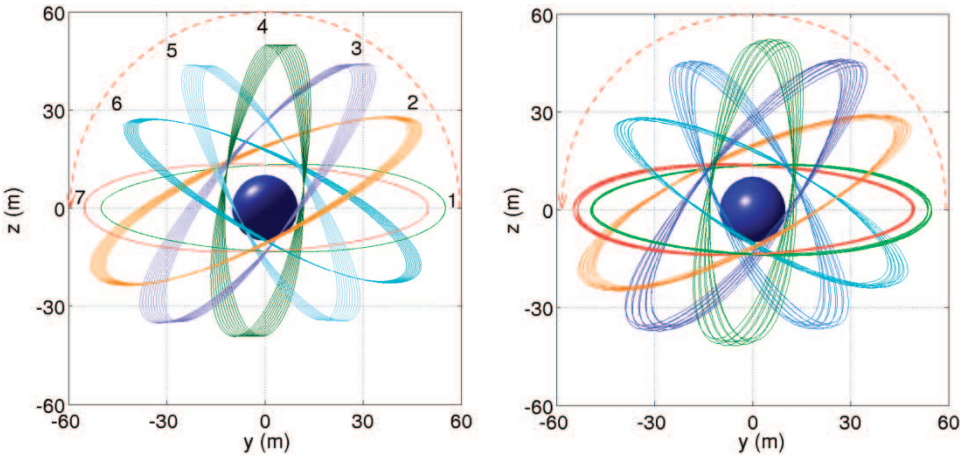

Figure 14. Variation in relative orbit expansion rate along the *yz*-plane.

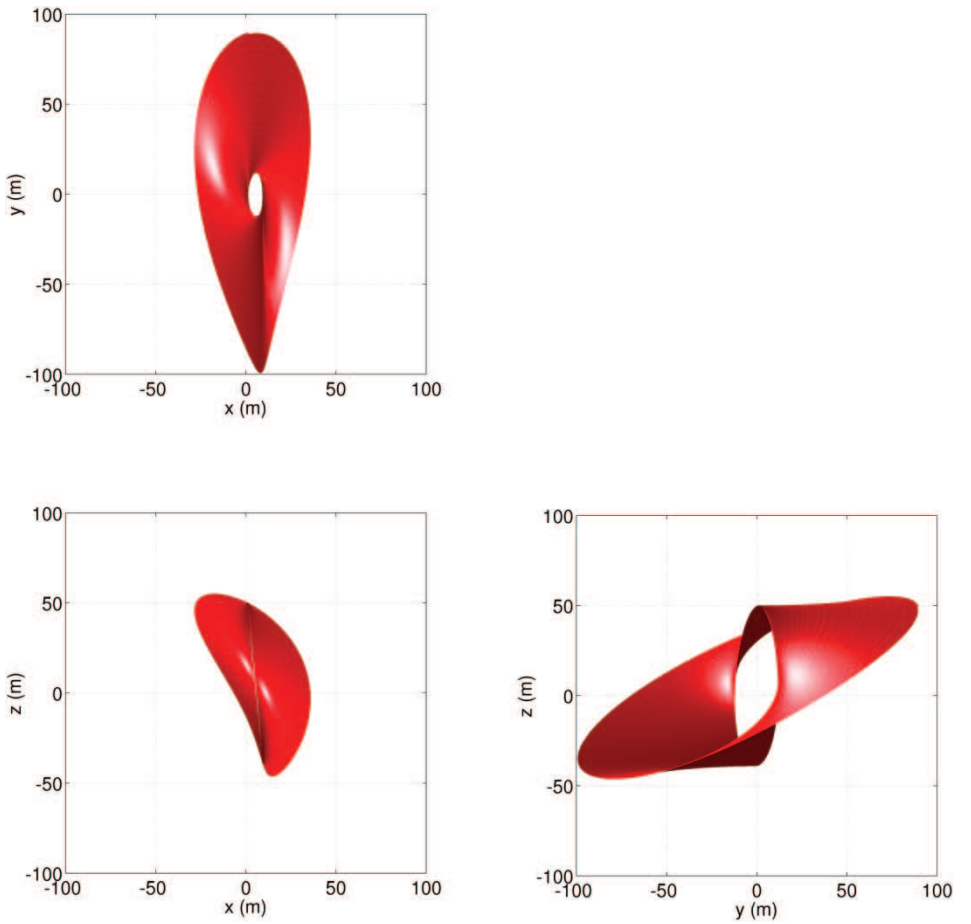

Figure 15. Evolution of nearly vertical orbit over 100 revolutions (49.2 years).

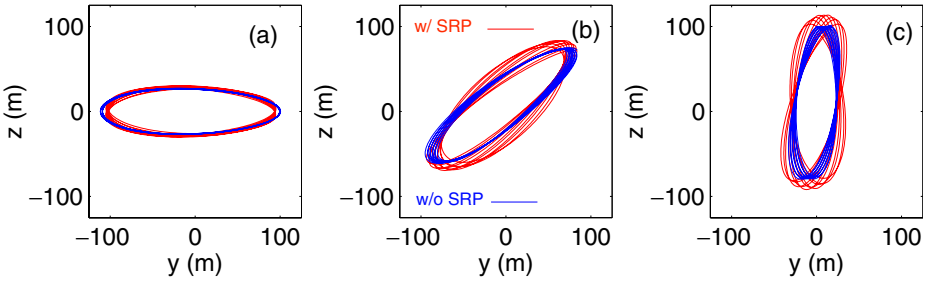

Figure 16. Natural formations in the EPHEM model (with SRP).

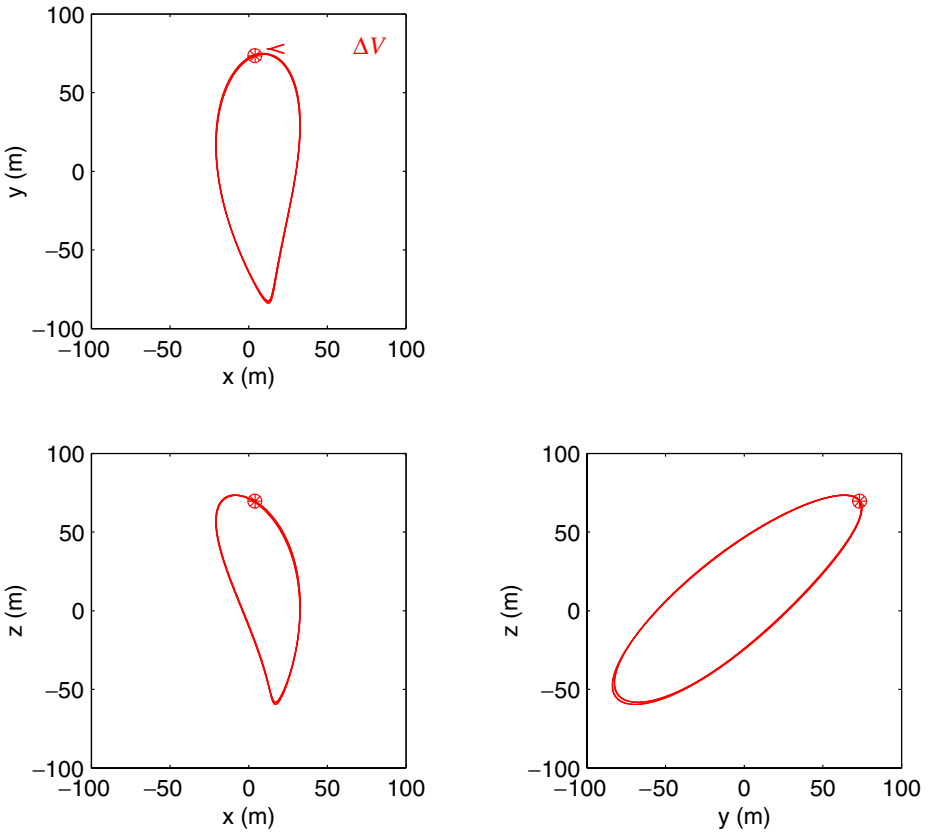

Figure 17. Controlled periodic orbit in the EPHEM model (without SRP).

process, in this case with initial- and end-point constraints, determines the manoeuvre necessary to close the orbit over this time period. The patch points associated with the converged solution are then shifted forward in time to add N additional revolutions. The complete solution is then differentially corrected while allowing manoeuvres at the intersections between revolutions. A sample solution, over six revolutions, is illustrated in figure 17 and is obtained by applying two impulsive manoeuvres ranging in size from 2.5 to 5 m s^{-1} at the specified locations.

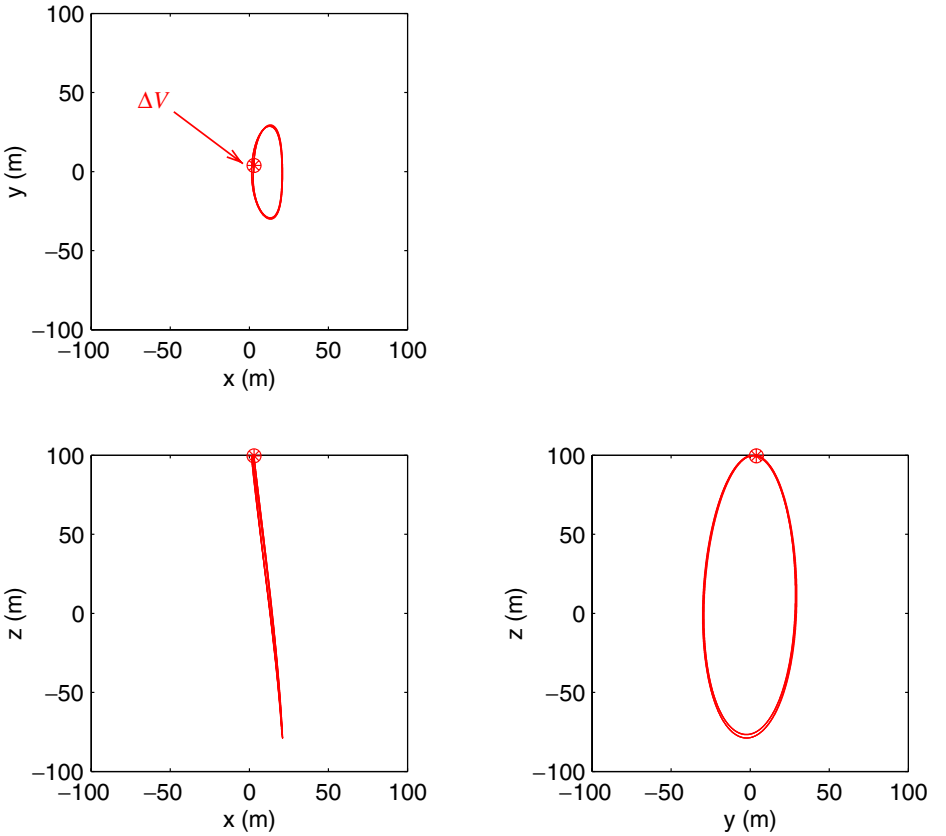

Figure 18. Controlled vertical orbit in the EPHEM model (without SRP).

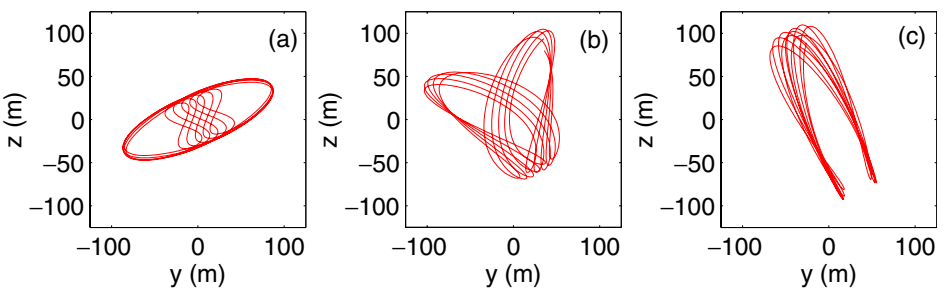

Figure 19. Natural formations in the EPHEM model (with SRP) (inertial frame perspective of figures 11(a–c)).

A similar approach can be applied to the nearly vertical trajectory in figure 16(c) to obtain vertical periodic relative orbits, as illustrated in figure 18. This particular approach works very well if periodicity is enforced in the rotating frame, as opposed to the inertial frame. Relative to an observer fixed in the rotating frame,

these solutions appear to be sufficiently close to periodic and are, subsequently, a suitable initial guess for the differential corrector. However, the associated inertial perspectives, illustrated in figure 19, are quite different. These solutions do not represent a sufficiently accurate initial guess if periodicity is the constraint to be enforced. That is because of the natural geometry of the solution and the fact that the Earth is at a different location every time a revolution is completed, as opposed to a perspective originating in the rotating frame. At the present time, however, no conclusive statements can be made since this is still a subject of ongoing study.

6. Conclusions

Earlier stages of this study demonstrate the efficiency of continuous control methods as applied to non-natural formations in the *n*-body problem. Although the results here include only the gravitational effects of the Sun, the Earth, and the Moon, it is important to note that the influence of the remaining planets is easily incorporated into this model. The addition of these perturbations, however, has an insignificant impact on the formation keeping problem near the libration points, L_1 and L_2, of the SEM system.

Based on the available literature on continuous control, it is clear that linear and nonlinear techniques, such as LQR and feedback linearization, can mathematically enforce a non-natural configuration in the *n*-body problem. However, continuous thruster operation does not always represent a desirable option. A difficulty inherent to the sensitive nature of this dynamical regime is that the acceleration levels required to maintain a non-natural configuration can be prohibitively small. Of course, whether or not this is true depends on the constraints imposed on the nominal formation dynamics.

Even with improved technology, the implementation error may be on the same order of magnitude as the thrust level, a potentially significant problem given the sensitivity of the dynamical response to small perturbations. Precise formations, in fact, may not even be required, given a possible shift to improved navigation and relative position information. Hence, it is useful to explore the effectiveness of discrete control.

For non-natural formations, a targeter approach is implemented here to maintain the desired configuration within a reasonable degree of accuracy. Not surprisingly, tightly spaced manoeuvres are required to closely maintain a desired non-natural configuration. The frequency of the manoeuvre interval depends on the desired nominal separation between each spacecraft and any additional dynamical constraints imposed on the formation. Furthermore, achieving the desired accuracy, and the physical requirements to do so, present yet another dilemma. As previously stated, if maintaining a tight non-natural formation is desired, frequent manoeuvres are necessary. However, smaller manoeuvre intervals require smaller manoeuvres. The magnitude of these manoeuvres, individually, is still extremely small which, once again, raises an implementation issue.

The difficulties encountered with non-natural configurations may be overcome by developing a better understanding of the naturally existing formations. Of course, a nominal configuration that is 'completely' consistent with the natural flow near

the reference orbit may not satisfy all the dynamical requirements imposed by a particular mission. However, understanding these naturally existing behaviours can lead to the development of techniques to aid the construction of nominal formations that do meet the proposed mission objectives, while exploiting the natural structure. To that end, a modified Floquet-based controller is successfully applied here that reveals some interesting natural formations as well as deployment into these configurations.

Acknowledgements

Any opinions, findings, and conclusions or recommendations expressed in this paper are those of the authors and do not necessarily reflect the views of the National Aeronautics and Space Administration. This research was carried out at Purdue University with support from the Clare Boothe Luce Foundation. It was also funded under Cooperative Agreement NCC5-727 through the NASA GSFC Formation Flying NASA Research Announcement.

References

[1] Micro Arcsecond X-Ray Imaging Mission (MAXIM) [Online]. Available at http://maxim.gsfc.nasa.gov
[2] Stellar Imager Homepage [Online]. Available at http://bires.gsfc.nasa.gov/~si/
[3] Terrestrial Planet Finder (TPF) [Online]. Available at http://planetquest.ipl.nasa.gov/TPF/tpf_index.html
[4] Terrestrial Planet Finder (TPF) Book [Online]. (May 1999) Available at http://planetquest.jpl.nasa.-gov/TPF/tpf_book/index.html.
[5] Vassar, R.H. and Sherwood, R.B., 1985, Eormationkeeping for a pair of satellites in a circular orbit. *Journal of Guidance, Control and Dynamics*, **8**, 235–242.
[6] Ulybyshev, Y., 1998, Long-term formation keeping of satellite constellation using linear quadratic controller. *Journal of Guidance, Control, and Dynamics*, **21**(1), 109–115.
[7] Chao, C.C., Pollard, J.E. and Janson, S.W., 1999, Dynamics and control of cluster orbits for distributed space missions. AAS/AIAA Space Flight Mechanics Meeting, 7–10 February 1999 (Breckenridge, CO: AAS), AAS Paper 99-126.
[8] de Queiroz, M.S., Kapila, V. and Yan, Q., 2000, Adaptive nonlinear control of multiple s/c formation flying. *Journal of Guidance, Control, and Dynamics*, **23**(3), 385–390.
[9] Kapila, V., Sparks, A.G., Buffington, J.M. and Yan, Q., 2000, Spacecraft formation flying: dynamics and control. *Journal of Guidance, Control, and Dynamics*, **23**(3), 561–563.
[10] Sparks, A., 2000, Satellite formationkeeping control in the presence of gravity perturbations. American Control Conference, 28–30 June 2000 (Chicago, IL: ACC).
[11] Stansbery, D.T. and Cloutier, J.R., 2000, Nonlinear control of satellite formation flight. AIAA Guidance, Navigation, and Control Conference and Exhibit, 14–17 August 2000 (Denver, CO: AIAA), AIAA Paper 2000-4436.
[12] Tan, Z., Bainum, P.M. and Strong, A., 2000, The implementation of maintaining constant distance between satellites in elliptic orbits. AAS/AIAA Space Flight Mechanics Meeting, 23–26 January 2000 (Clearwater, FL: AAS), pp. 667–683.
[13] Wang, Z., Khorrami, F. and Grossman, W., 2000, Robust adaptive control of satellite formationkeeping for a pair of satellites. American Control Conference, 28–30 June 2000 (Chicago, IL: ACC).
[14] Yan, Q., Yang, G., Kapila, V. and de Queiroz, M.S., 2000, Nonlinear dynamics nad output feedback control of multiple spacecraft in elliptic orbits. American Control Conference, 28–30 June 2000 (Chicago, IL: ACC).
[15] Yedevalli, R.K. and Sparks, A.G., 2000, Satellite formation flying control design based on hybrid control system stability analysis. American Control Conference, 28–30 June 2000 (Chicago, IL: ACC).

[16] Irvin, D.J. Jr. and Jacques, D.R., 2001, Linear vs. nonlinear control techniques for the reconfiguration of satellite formations. AIAA Guidance, Navigation, and Control Conference and Exhibit, 6–9 August 2001 (Montreal, Canada: AIAA), AIAA Paper 2001-4089.
[17] Sabol, C., Burns, R. and McLaughlin, C., 2001, Satellite formation flying design and evolution. *Journal of Spacecraft and Rockets*, **38**(2), 270–278.
[18] Schaub, H. and Alfriend, K.T., 2001, Impulsive spacecraft formation flying control to establish specific mean orbit elements. *Journal of Guidance, Control, and Dynamics*, **24**(4), 739–745.
[19] Starin, S.R., Yedavalli, R.K. and Sparks, A.G., 2001, Spacecraft formation flying manoeuvers using linear quadratic regulation with no radial axis inputs. AIAA Guidance, Navigation, and Control Conference and Exhibit, 6–9 August 2001 (Montreal, Canada: AIAA), AIAA Paper 2001-4029.
[20] Vadali, S.R., Vaddi, S.S., Naik, K. and Alfriend, K.T., 2001, Control of satellite formations. AIAA Guidance, Navigation, and Control Conference and Exhibit, 6–9 August 2001 (Montreal, Canada: AIAA), AIAA Paper 2001-4028.
[21] Simó, C., Gómez, G., Llibre, J., Martinez, R. and Rodriguez, J., 1987, On the station keeping control of halo orbits. *Acta Astronautica*, **15**(6/7), 391–397.
[22] Howell, K.C. and Keeter, T., 1995, Station-keeping strategies for libration point orbits—target point and Floquet mode approaches. *Advances in the Astronautical Sciences*, **89**(2), 1377–1396.
[23] Barden, B.T. and Howell, K.C., 1998a, Formation flying in the vicinity of libration point orbits. *Advances in Astronautical Sciences*, **99**(2), 969–988.
[24] Barden, B.T. and Howell, K.C., 1998b, Fundamental motions near collinear libration points and their transitions. *The Journal of the Astronautical Sciences*, **46**(4), 361–378.
[25] Barden, B.T. and Howell, K.C., 1999, Dynamical issues associated with relative configurations of multiple spacecraft near the Sun–Earth/Moon L_1 point. AAS/AIAA Astrodynamics Specialists Conference, 16–19 August 1999 (Girdwood, AK: AAS), AAS Paper 99-450.
[26] Howell, K.C. and Barden, B.T., 1999, Trajectory design and stationkeeping for multiple spacecraft in formation near the Sun–Earth L_1 point. IAF 50th International Astronautical Congress, 4–8 October 1999 (Amsterdam, the Netherlands: IAF/IAA), IAF/IAA Paper 99-A707.
[27] Folta, D., Carpenter, J.R. and Wagner, C., 2000, Formation flying with decentralized control in libration point orbits. International Symposium: Spaceflight Dynamics, June 2000 (Biarritz, France).
[28] Scheeres, D.J. and Vinh, N.X., 2000, Dynamics and control of relative motion in an unstable orbit. AIAA/AAS Astrodynamics Specialist Conference, 14–17 August 2000 (Denver, CO: AIAA), AIAA Paper 2000-4135.
[29] Gómez, G., Lo, M., Masdemont, J. and Museth, K., 2001, Simulation of formation flight near Lagrange points for the TPF mission. AAS/AIAA Astrodynamics Conference, 30 July–2 August 2001 (Quebec, Canada: AAS), AAS Paper 01-305.
[30] Gurfil, P. and Kasdin, N.J., 2001, Dynamics and control of spacecraft formation flying in three-body trajectories. AIAA Guidance, Navigation, and Control Conference and Exhibit, 6–9 August 2001 (Montreal, Canada: AIAA), AIAA Paper 2001-4026.
[31] Hamilton, N.H., 2001, Formation flying satellite control around the L_2 Sun–Earth libration point. MS thesis, George Washington University, Washington, DC.
[32] Luquette, R.J. and Sanner, R.M., 2001, A non-linear approach to spacecraft formation control in the vicinity of a collinear libration point. AAS/AIAA Astrodynamics Conference, 30 July–2 August 2001 (Quebec, Canada: AAS), AAS Paper 01-330.
[33] Gurfil, P., Idan, M. and Kasdin, N.J., 2002, Adaptive neural control of deep-space formation flying. American Control Conference, 8–10 May 2002 (Anchorage, AK: ACC), pp. 2842–2847.
[34] Howell, K.C. and Marchand, B.G., 2003, Control strategies for formation flight in the vicinity of the libration points. AAS/AIAA Space Flight Mechanics Conference, 9–13 February 2003 (Ponce, Puerto Rico: AAS), AAS Paper 03-113.
[35] Marchand, B.G. and Howell, K.C., 2003, Formation flight near L_1 and L_2 in the Sun–Earth/Moon ephemeris system including solar radiation pressure. AAS/AIAA Astrodynamics Specialists Conference, 3–8 August 2003 (Big Sky, MT: AAS), AAS Paper 03-596.
[36] Marchand, B.G. and Howell, K.C., 2004, Aspherical formations near the libration points of the Sun–Earth/Moon system. AAS/AIAA Space Flight Mechanics Meeting, 7–12 February 2004 (Maui, HI: AAS), AAS Paper 04-157.
[37] McInnes, C.R., 1999, *Solar Sailing: Technology, Dynamics and Mission Applications*, *Springer–Praxis Series in Space Sciences and Technology* (UK: Praxis Publishing Ltd.).
[38] Mueller, J., 1997, Thruster options for microspacecraft: a review and evaluation of existing hardware and emerging technologies. 33rd AIAA/ASME/SAE/ASEE Joint Propulsion Conference and Exhibit, 6–9 July 1997 (Seattle, WA: AIAA), AIAA Paper 97-3058.
[39] Gonzales, A.D. and Baker, R.P., 2001, Microchip laser propulsion for small satellites. 37th AIAA/ASME/SAE/ASEE Joint Propulsion Conference and Exhibit, 8–11 July 2001 (Salt Lake City, UT: AIAA), AIAA Paper 2001-3789.

[40] Phipps, C. and Luke, J., 2002, Diode laser-driven microthrusters—a new departure for micropropulsion. *AIAA Journal*, **40**(2), 310–318.
[41] http://space-power.grc.nasa.gov/ppo/projects/eo1/eo1-ppt.html
[42] Nayfeh, A.H. and Mook, D.T., 1979, *Nonlinear Oscillators* (New York: John Wiley).
[43] Howell, K.C. and Pernicka, H.J., 1988, Numerical determination of Lissajous trajectories in the restricted three-body problem. *Celestial Mechanics*, **41**, 107–124.